

CHALMERS



Radio emission towards Eta Carinae

Master of Science Thesis in the Master Degree Programme, Radio and Space Science

MARGIT RÄSTAS

Department of Earth and Space Science
Division of Astrophysics
CHALMERS UNIVERSITY OF TECHNOLOGY
Göteborg, Sweden 2011
Report No. xxxx

ABSTRACT

Eta Carinae with its peculiar surrounding has been a mystery for decades despite numerous surveys carried out. In this paper we focus on a H26 α emission line in order to find out if the results will shed some light on the subject.

In order to have a clearer picture of Eta Carinae the earlier work published on the studies of the object has been summarized in the introduction. Before going deeper into the studies some theories are explained that are essential to understand the analysis done in the second part of the paper. The theories include local thermodynamic equilibrium (LTE) conditions applied to the medium in order to determine the line-to-continuum intensity ratio which yields an estimate of electron temperature of the emitting region. This value is necessary for the subsequent model calculations. The departures from LTE are also relevant to understand and have been discussed in separate section.

For the analysis we have assumed the emission to originate from ionized wind and therefore a simplified spherically symmetric wind model with uniform mass loss rate has been described as well as applied. It is clear that the actual structure of the wind may strongly deviate from the model though. The spectral energy distribution (SED) of Eta Carinae discussed in the section describes the origin of the continuum emission. Since the analyzed line profile is showing broadening effect in the wings another section is dedicated to a possible broadening theory – Stark effect. Some rather interesting results from earlier studies on some recombination lines towards Eta Carinae claiming a maser emission have been discussed in a separate section.

In the final section we give the description of data and its analysis with MATLAB. First we notice that the He/H ratio is out of the ordinary. When concentrating on H26 α line we try to see the similarities/discrepancies between the observed line profile and the profile we obtain by using the simple wind model. The terminal velocity of the wind has been estimated in different ways resulting in differences in line profiles expected from the simple model of wind in LTE. All of those however are surprisingly low for such a massive star. To account for the line wing broadening the impact broadening effect is applied to the modeled profile which for one specific modified case gives a rather good fit. Since there has been an abrupt change over a short period of time observed in the line intensities lately we have also tried to estimate the timescale for the recombination.

TABLE OF CONTENTS

1. INTRODUCTION.....	1
2. THEORIES ESSENTIAL FOR ANALYSIS.....	4
2.1 Formation of Hydrogen Radio Recombination Lines and the Underlying Continuum.....	4
2.2 Line Intensity and Electron Temperature of HII Regions Under LTE Conditions.....	5
2.3 Departures From LTE.....	10
2.3.1 Line Intensities in Non-LTE Conditions.....	10
2.3.2 The Theory of Maser.....	14
2.4 Stellar Wind and Spectral Energy Distribution.....	16
2.5 Line Broadening by the Stark Effect.....	21
2.6 Maser Emission Detection in Millimeter Recombination Lines Towards Eta Carinae. . .	24
3. WORKING WITH DATA.....	27
3.1 The Observations.....	27
3.2 Data Analysis.....	27
3.2.1 Fitting the Line Profile and Comparing It to the Results Obtained from Simple Wind Model in LTE.....	27
3.2.2 LTE Line Profile with Broadening Effect.....	35
3.2.3 Changes in the Line Intensities.....	38
4. CONCLUSIONS.....	40
REFERENCES.....	41

1. INTRODUCTION

Eta Carinae with its luminosity of $\sim 10^6 L_{\odot}$ is one of the most luminous and massive evolved stars in the Milky Way galaxy that is close enough (~ 2.35 kpc) to be observed and studied in detail. Despite all the studies carried out the understanding of Eta Carinae still remains quite poor (Davidson & Humphreys 1997).

It is a star famous for its great instability features. It has undergone and survived an enormous non-thermal stellar explosion called “the Great Eruption” in 1840s which was comparable to a supernova event in terms of luminous energy output. During this eruption a few solar masses of gas was expelled which has formed into a bipolar nebula now called the Homunculus. There is also a number of features which seem to be ejected later possibly during subsequent eruption. Those eruptive events have formed a large amount of dust and ejected matter with elemental abundances that are thought to be out of the ordinary. The Homunculus nebula with its proximity and physical characteristics provides us with perfect laboratory helping us to study a number of physical processes in the interstellar medium.

Some of the earlier work has provided us with detailed images displaying the bipolar nebula with its surface appearing clumpy and the ragged equatorial disk. The polar lobes have been described as two osculating spheroids which due to the limb brightening in optical and mid-IR maps were said to be hollow (Smith 2006). At UV and visual wavelengths the Homunculus is mainly seen as a reflection nebula. Most of the radiation from the central star is absorbed by the surrounding dust and reradiated in thermal IR (Smith & Ferland 2007). The studies of near-IR spectra showed a double-shell structure for the lobes where most of the mass is in geometrically thinner outer molecular shell seen in near-IR H_2 emission and about 10% of it is in the inner shell of partially ionized atomic gas seen in optical and near-IR [Ni II] and [Fe II] emission. Thermal-IR imaging showed that the inner shell of dust has a temperature of ~ 200 K while the outer shell of cooler dust is ~ 140 K. Based on fits of the IR spectral energy distribution the masses for the inner and outer shell are derived to be $1.5 M_{\odot}$ and $11 M_{\odot}$ respectively with a gas-to-dust mass ratio of ~ 100 . (Smith et al. 2003b). On the other hand Gomez et al. (2010) have estimated, based on sub-millimeter studies, that the ejected mass is more than $40 M_{\odot}$ which is almost three times larger than the one estimated using IR data. The densities for neutral H are found to be $n_H \approx 10^{5.5} \text{ cm}^{-3}$ and $n_H \approx (0.5-1) \cdot 10^7 \text{ cm}^{-3}$ in the inner shell

and outer shell respectively to permit H_2 and Fe^0 to “survive” simultaneously. The derived density and known size of the nebula give an independent result for the total mass which agrees with the one derived from IR spectra yielding that the gas-to-dust mass ratio can be considered close to the normal value of 100 (Smith & Ferland 2007). A later addition is a smaller bipolar nebula called the Little Homunculus inside the Homunculus which, indicated by the historical lightcurve, was most likely ejected in a secondary eruption during 1890s. It is orientated along the same bipolar axis but it appears to be stretched horizontally compared to the Homunculus probably because of following a different expansion law (Fig. 1). The estimated densities in the Little Homunculus range from $10^4 - 10^7 \text{ cm}^{-3}$ and its mass is estimated to be about $0.1 M_{\odot}$ (Smith 2009).

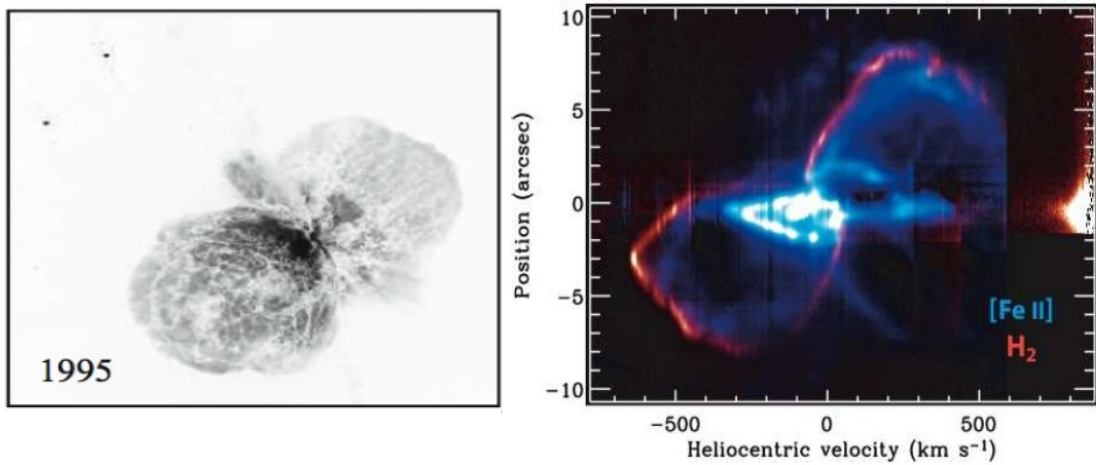


Fig. 1 *Left*: A red-wavelength image of the Homunculus showing the clumpy surface and ragged equatorial disk. *Right*: IR image of Homunculus showing the shape and detailed double-shell structure in H_2 (red thin outer shell) and $[\text{FeII}]$ (blue thicker inner shell) (Smith 2009).

The central star itself is hidden from our view by the ejected matter but it has commonly been classified as an extreme case of luminous blue variable (LBV) star with mass of $100 M_{\odot}$ (Smith et al. 2003b). LBVs are known to have high luminosity, great instability and periods of high mass loss rate (Clark et al. 2005). Eta Carinae's mass loss rate is estimated to be $10^{-4} - 10^{-3} M_{\odot}$ per year or even as high as $10^{-2} M_{\odot}$ in the recent studies by Gomez et al. (2010). An episodic mass loss introducing a change in the number of ionizing photons could be one

way to explain the variability of the radio cycle (Smith et al 2003a; Gomez et al. 2010). It has also been discussed that the star might have a binary companion which would explain the extreme mass loss and strong radio variability with 5.5 year cycle (Cox et al. 1995a). The periodicity of variability suggests that the orbit of the binary is highly eccentric causing intense wind-wind collisions. Attempts to attribute the bipolar structure and the present day fast polar wind to interaction with binary companion have been made (Soker et al. 2004). The origin of the shape of the Homunculus is still unknown but could be explained as well by a mass ejection into a non-uniform interstellar medium (ISM) where the ISM in the equatorial plane is pictured to be denser than in the direction of the poles (Gomez et al. 2006).

Besides infrared emission Eta Carinae is also an outstanding radio, millimeter and even X-ray source. The studies of near-IR to decimeter radio range have shown that millimeter emission of Eta Carinae is dominated by thermal emission from the ionized thermal wind (Gomez et al. 2010). It has often been reported that some millimeter radio recombination lines towards Eta Carinae are resulting from maser emission (microwave amplification by the stimulated emission) since the recombination lines show a strong blue-shifted peak overlying a broad weaker component and the line intensity ratios of β to α lines are small. Strong maser action is rare in observations of radio recombination lines and so far appeared only in the stellar wind and ionized disk of MWC 349 (Cox et al. 1995a).

In current project we are particularly interested in figuring out if the aforementioned maser emission prediction applies to an observed hydrogen line or is it merely quasi-thermal but very intense. For that purpose a data-set of (sub)millimeter observation of H 26α and He 26α lines towards Eta Carinae will be analyzed. The observed intensity of H 26α line combined with the intensity of the continuum emission is used to determine the electron temperature under LTE condition. A model calculation of expected line profile under LTE conditions will then be compared to the observed line profile. A number of different approaches are applied to explain the deviation of the observed line profile from the one expected from simple model of wind in LTE with an attempt to figure out some of the properties of emitting region and possibly find out the source of emission.

2. THEORIES ESSENTIAL FOR ANALYSIS

2.1 Formation of Hydrogen Radio Recombination Lines and the Underlying Continuum

Radio recombination lines (RRLs) of hydrogen are spectral lines in the radio frequency domain. These lines arise from ionized hydrogen (HII) regions that lie closer to the ionizing source. Radio recombination lines can provide important information on the physical state of the ionized circumstellar gas like that of Eta Carinae's itself that generally is not possible to obtain with other observational means. Radio recombination lines can provide radial velocity, electron temperature, electron density and relative abundances of other ionized atoms present in the gas. All these properties are important to understand the structure of a nebula (Dupree & Goldberg 1970).

Thermal radio sources forming radio recombination lines are often close to local thermodynamic equilibrium (LTE). In LTE the excited electronic state populations are described by Boltzmann distribution¹. In order for LTE to hold the rate of radiative transfer into one specific level must be balanced by the rate of radiative transfer out of the same level. The same applies for the rate of collisions thermalizing the gas (*“Radio Recombination Lines: Their Physics and Astronomical Applications”*, s. 2.3).

The HII regions are photo-ionized plasmas that are almost fully ionized. There still exists a fraction of neutral hydrogen atoms which can be ionized by ultraviolet photons. The inverse process also occurs, where an ion and an electron are turned into one particle and is called radiative recombination. After recombining the atom is often in a highly excited state. The time interval between two subsequent ionizations of the same atom is generally longer than the time for the recombined atom to cascade down to its ground state. The electron cascading down the energy levels emits photons to conserve energy. The frequency of the emitted photon depends on the energy levels between which the transition takes place. Transitions between high energy states are responsible for the radio emission lines we see in the observed spectra (*“Tools of Radio Astronomy”*, ch. 14).

¹ $p(n) = 2n^2 \exp(-E_n/kT)$ where the energy of a Rydberg state n is $E_n = R(1 - 1/n^2)$ for Rydberg constant R .

Since the line emission lies on top of continuum emission that also contributes to the intensity of the line peak and it must be taken into account. Continuum emission from HII regions is a mixture of thermal emission from the heated dust and the so called free-free radiation or Bremsstrahlung from unbounded charged particles. Ultraviolet radiation from the central source heats the dust and ionizes the gas. Usually continuum emission at radio frequencies mostly comes from free-free transitions. It can be described as a freely moving electron in plasma that comes sufficiently close to an ion and is thereby accelerated. In the acceleration process the electron radiates a photon to conserve the energy. The ionized gas particles are free and have no quantized energy levels therefore the free-free radiation is continuous over the spectrum. The dust emission is similar to black body spectrum. At shorter wavelengths from the peak the emission is optically thick but at longer wavelengths from the peak it can be optically thin in the millimeter wavelength range. At very high frequencies the dust emission can become stronger than free-free emission (“*Radio Recombination Lines: Their Physics and Astronomical Applications*”, s. 2.3). Some of the recent studies have given the spectral energy distribution (SED) of Eta Carinae from near infrared to radio wavelengths (Fig. 5) (Cox et al. 1995b; Gomez et al. 2010).

Because of the long wavelengths of radio line emission they are unaffected by interstellar dust. Therefore the radio recombination lines can be used to explore the galactic HII regions in the way that is not possible at other smaller wavelengths. However LTE does not apply to all recombination lines thus their interpretation may be complicated by non-LTE effects (“*The Physical Universe: An Introduction to Astronomy*”, ch. 11; “*Radio Recombination Lines: Their Physics and Astronomical Applications*”, s. 3.1).

2.2 Line Intensity and Electron Temperature of HII Regions Under LTE Conditions

Information on electron temperature T_e and electron density n_e in gaseous nebula can be obtained from the measurements of radio recombination lines. The populations of the high levels of hydrogen depend on T_e and n_e and the strength of the lines emitted by transitions between those levels relative to continuum and to each other are dependent on T_e , n_e and optical depth τ_ν , which is described below in detail. Thus the observed and calculated relative strengths

of the recombination line can be used to calculate T_e and n_e (“*Astrophysics of Gaseous Nebulae and Active Galactic Nuclei*”, s. 5.8).

Here we consider an idealized homogeneous isothermal nebula. The rest frequency of a recombination line produced by transition from upper level of principal quantum number n' to a lower level n'' is given in GHz by the empirical equation:

$$\nu_{n'n''} = c R_M Z^2 \left((n')^{-2} - (n'')^{-2} \right) \quad (1)$$

where c is the speed of light, Z is the charge of the atom or ion as seen by the highly excited electron and R_M for atom of mass M is given by the equation:

$$R_M = \frac{R_\infty}{1 + m_e / M} \quad (2)$$

where R_∞ is Rydberg's constant. Approximating equation (1) for frequency in the case where the quantum number of the lower state is high enough ($n'' \gg 1$) and the difference between the quantum numbers of the states is small enough ($\Delta n \ll n''$) will take the following form:

$$\nu_{n'n''} \approx c R_M Z^2 \frac{2 \Delta n}{(n'')^3} \quad (3)$$

We are interested in finding both the line radiation and the continuum radiation intensities at the same frequency. To do so we start from giving solution to the equation of radiative transfer which has to cover both of the line and continuum emissions, since continuum radiation is not weak compared to the line radiation. The solution in axial direction is

$$\frac{dI_\nu}{ds} = -\kappa_\nu I_\nu + j_\nu \quad (4)$$

where κ_ν and j_ν are absorption coefficient and volume emissivity of the gas respectively. The specific intensity I_ν of the radiation at a specific frequency is the sum of line radiation intensity and continuum radiation intensity. The absorption coefficient is position dependent but for a

simplified model it can be taken to be constant in every position. It can be written to a more convenient physical form by using its relation with optical depth of the radiation.

$$d\tau_v = \kappa_v ds \quad (5)$$

which can be substituted in the radiative transfer equation and that gives the solution of the latter in the following form

$$I_v = I_c + I_l = I_v(0) \exp(-\tau_v) + \int_0^{\tau_v} \frac{j_v}{\kappa_v} \exp(-(\tau_v - \tau_v')) d\tau_v' \quad (6)$$

where I_c and I_l are observed intensities of continuum and line, respectively. $I_v(0)$ stands for the intensity of the background radiation of a specific frequency entering the medium. The term containing $I_v(0)$ can be neglected when the background radiation is weak compared with the emission of the nebula itself. Using Kirchoff's law of thermodynamics gives the relation between emission coefficient and absorption coefficient in LTE

$$\frac{j_v}{\kappa_v} = B_v(T_e) \quad (7)$$

where $B_v(T_e)$ is Planck function at electron temperature T_e . Now integrating equation (6) and inserting equation (7) will give the specific intensity of the radiation emerging from the medium in a convenient form

$$I_v = I_c + I_l = B_v(T_e)(1 - \exp(-\tau_v)) \quad (8)$$

The solution of the radiative transfer equation for continuum radiation in LTE is of similar form

$$I_c(\nu) = B_\nu(T_e)(1 - \exp(-\tau_c(\nu))) \quad (9)$$

where τ_c is the optical depth of the free-free radiation. The Planck function at electron temperature T_e in terms of frequency is given by

$$B_\nu(T_e) = \frac{2h\nu^3}{c^2} \frac{1}{\exp(h\nu/kT_e) - 1} \quad (10)$$

Since the specific intensity is equal to the Planck function at brightness temperature $T_b(\nu)$, equation (8) is equivalent to

$$T_b(\nu) = T_l + T_c = T_e \left(1 - \exp(-\tau_l(\nu) - \tau_c(\nu)) \right) \quad (11)$$

at frequencies where $h\nu \ll kT_e$ where the total optical depth of the radiation at the line center is the sum of line and continuum opacities $\tau_l(\nu)$ and $\tau_c(\nu)$ respectively. The optical depth of the free-free radiation at radio frequencies for homogeneous isothermal region of size s is given by Dupree & Goldberg (1970)

$$\tau_c = 0.08235 a(\nu, T_e) T_e^{-1.35} \nu_{\text{GHz}}^{-2.1} E_c \quad (12)$$

where E_c is the continuum emission measure given by integral of the product of electron number density n_e and ion number density n_i over the path length through the nebula $\int n_e n_i ds$ in units of $[\text{cm}^{-6} \text{ pc}]$ and $a(\nu, T_e)$ is weakly varying function which at temperatures near 10^4 K is approximately unity over the entire radio spectrum.

$$\tau_l = 1.006 \cdot 10^7 Z^2 \Delta n f_{n''n'} / n'' T_e^{-5/2} \exp(X_n) E_l / \Delta \nu \quad (13)$$

The optical depth τ_l in the line center in LTE is given also by Dupree & Goldberg (1970). The oscillator strength for the alpha lines is $f_{n''n'} \approx 0.1908n''$. The factor $X_n = 157801/n^2 T_e$ is the ratio of the energy of the state n'' to kT_e but at temperatures of HII regions the exponential factor containing this ratio approaches unity and therefore can be neglected. E_l is the corresponding line emission measure of the recombining ion which to a good approximation for hydrogen can be taken equal to the continuum emission measure E_c assuming that both the line and continuum emission at given frequency are coming approximately from the same region (Dupree & Goldberg 1970). If the line profile is assumed to have a Gaussian form the full-width at half-maximum can be given as $\Delta \nu = \nu \Delta V/c$ in kHz.

Let us now substitute the temperatures with the intensities also in equation (9) to obtain the intensity rising from continuum emission. By subtracting the result from equation (11) after which dividing it by equation (11) we will finally get to the line-to-continuum intensity ratio equation

$$\frac{T_l}{T_c} \Delta \nu = \frac{1 - \exp(-\tau_l)}{1 - \exp(-\tau_c)} \Delta \nu \quad (14)$$

Since expanding $1 - \exp(-x)$ by Taylor series results in x in case $x \ll 1$ the same approach can be used here. In optically thin gas when both optical depths are very small, $\tau_c \ll 1$ and $\tau_l \ll 1$, the line-to-continuum intensity ratio for alpha transitions ($\Delta n = 1$) can be written as follows:

$$\frac{T_l}{T_c} \Delta \nu = 2.33 \cdot 10^4 T_e^{-1.15} \nu_{GHz}^{2.1} \quad (15)$$

The line-to-continuum intensity ratio is often observed and it yields an estimate of electron temperature T_e independent of emission measure as long as the frequency is high enough so that the opacities of the line and continuum are small (Dupree & Goldberg 1970). Equation (15) is applicable for medium of pure hydrogen only. In the current case helium contributes to the continuum emission but not to the hydrogen line emission. To correct this for present case an additional factor of 1.08^{-1} for the mentioned effect must be added².

Substituting $\Delta V = \Delta \nu c / V$ we now arrive to the equation for electron temperature

$$T_e = \left[6.985 \cdot 10^3 \nu_{GHz}^{1.1} \cdot 1.08^{-1} \left(\frac{T_l}{T_c} \right)^{-1} \Delta V^{-1} \right]^{0.87} [K] \quad (16)$$

In this equation for the electron temperature the impact broadening is assumed to be negligible. Since it is claimed that this effect becomes important at high n lines the resulting equation can be considered applicable.

It should also be reminded that the approach described is applicable to a nebula of

2 The average He^+/H^+ ion ratio is $N(\text{He}^+)/N(\text{H}^+) \approx 0.08$ when helium is ionized to the same extent as hydrogen. Helium ions contribute to continuum emission but not to the line emission, therefore $N(\text{H}^+)/[N(\text{He}^+)+N(\text{H}^+)] = 1.08^{-1}$.

homogeneous and isothermal structure where helium is singly ionized. Its advantage is that the estimate of the electron temperature is obtainable from limited data, furthermore it is the only nebular model that allows to analytically reduce the expression of T_i/T_e so that the electron temperature of the gas can be estimated. Several approximations have been made here among which most importantly the dependence of T_i/T_e on the density of the nebula and on the path length through the nebula have been removed. The correct expression for T_i/T_e has a specific dependence on both the aforementioned factors. Using equation (16) shows the changes of the density of the nebula and the path length through the nebula as apparent changes in temperature (Brown & Lockman 1978).

2.3 Departures from LTE

2.3.1 Line Intensities in Non-LTE Conditions

Even though the assumption of LTE for galactic HII regions is assumed to be generally a good one there still occur departures from LTE and those cases need to be treated differently. Since the excited electronic state populations are described different from the Boltzmann distribution the absorption coefficient and emissivity must be defined in another way taking into account the aforementioned fact. The departure coefficients $b_{n'}$ and $b_{n''}$ plus correction coefficient $\beta_{n'n''}$ for stimulated emission are therefore introduced.

The departure coefficient $b_{n'}$ is the ratio of the actual population $N_{n'}$ of the upper level n' to the one that is given by Saha-Boltzmann equation³. The stimulated emission in the line is also an important aspect and must be taken into account when redefining the absorption coefficient. Figure 2 gives an instructive picture of how the departure coefficient and amplification factor depend on different conditions. The results correspond to a range of electron densities at fixed electron temperature of $T_e = 10^4$ K. The upper panel shows that in a dense medium where level populations are dominated by collisional rates the departure

³
$$\frac{N(H^+)N(e)}{N_n(H)} = \frac{2g_{H^+}}{g_n} \left(\frac{2\pi m k T}{h^2} \right)^{3/2} \exp\left(-\frac{h\nu}{kT}\right)$$
 describes the population of state n of the atom relative to the numbers of recombining electrons and ions. The factors g are the corresponding statistical weights.

coefficient approaches the value of 1 since the relative populations of bound levels are well described by electron temperature T_e , but in sparse medium dominated by radiative rates this description of populations does not hold so well and the values for departure coefficients start to have smaller values than 1. With the decreasing principal quantum number the atomic radius

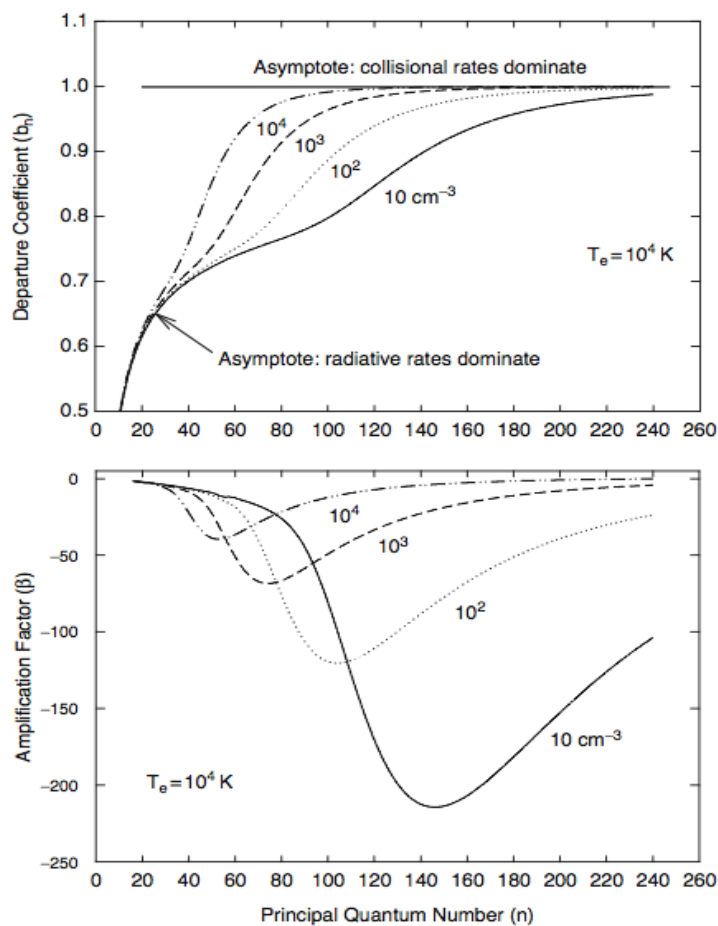


Fig. 2 *Top panel:* departure coefficients for the principal quantum levels of hydrogen for a range of electron densities. (The Lyman lines of the medium are assumed to be optically thick, all the other lines optically thin - “Case B”) *Bottom panel:* The corresponding correction term for stimulated emission α type RRLs plotted in the form of β . (“Radio Recombination Lines: Their Physics and Astronomical Applications”, s. 2.3)

decreases and along with it the influence of collisions so the departure coefficient correspondingly lie below 1. The lower panel shows that the lowest correction for stimulated

emission and hence the largest amplification of the line occurs at lower densities. This is due to the slope of departure coefficient $d\ln b_n/dn$ being inversely weighted by the photon energy $h\nu$ in the equation for correction term β (“*Radio Recombination Lines: Their Physics and Astronomical Applications*”, s. 2.3; Dupree & Goldberg 1970; Brown & Lockman 1978)⁴. The values for both the departure coefficients $b_{n'}$ and correction coefficient $\beta_{n''n'}$ have been calculated and tabulated among others in paper by Walmsley (1990). However it is necessary to mention that due to the extraordinary environment of Eta Carinae those coefficients tabulated in papers mentioned above can give rather unreliable results. The reason for this is that none of those papers have included non-LTE effects due to a strong far-IR continuum. Since Eta Carinae is an extremely strong IR source, in fact it is the brightest IR source outside the Solar system, those coefficients would have to be recalculated in case of detecting non-LTE conditions.

To redefine the volume emissivity of the gas in case of departure from LTE the Kirchoff's law of thermodynamics used in equation (7) has to be modified taking into account the departure coefficient which accounts for the non-LTE line formation effect, thus

$$j_\nu = j_c + j_l = B_\nu(T_e)(\kappa_c + b_{n'}\kappa_l') \quad (17)$$

where κ_c is the continuous absorption coefficient and κ_l' is the central line absorption coefficient in LTE. The non-LTE correction factors apply only to the line coefficients because the electron temperature T_e describes the thermodynamic state of the ionized gas and the continuum coefficients do not need any correction. The absorption coefficient κ_ν takes the following form:

$$\kappa_\nu = \kappa_c + \kappa_l = \kappa_c + b_{n''}\beta_{n''n'}\kappa_l' \quad (18)$$

Now the determination of line intensities can be approached in a similar way as before. Using equations (17) and (18) the solution to radiative transfer equation can be written as

4 According to Dupree and Goldberg (1970) the correction term β is defined by

$$\beta_{n''n'} \approx \frac{b_{n'}}{b_{n''}} \left[1 - \left(\frac{kT_e}{h\nu} \right) \left(\frac{d\ln b_{n''}}{dn} \right) \Delta n \right] \quad \text{where } \Delta n = n' - n''.$$

$$I_v = I_c + I_l = B_v(T_e) \frac{\kappa_c + b_{n'} \kappa_l'}{\kappa_c + b_{n''} \beta_{n''n'} \kappa_l'} (1 - \exp(-\tau_v)) \quad (19)$$

To obtain the line-to-continuum intensity ratio the equation for continuum intensity (9) must be subtracted from the above equation (19) and the result must be divided by the same equation for continuum intensity. The intensities can be again substituted by temperatures. This yields

$$\frac{I_l}{I_c} = \frac{T_l}{T_c} = \eta_v \frac{1 - \exp(-\tau_v)}{1 - \exp(-\tau_c)} - 1 \quad (20)$$

where η_v is a correction factor for the Planck function in cases of departures from LTE and is given by

$$\eta_v = \frac{\kappa_c + b_{n'} \kappa_l'}{\kappa_c + b_{n''} \beta_{n''n'} \kappa_l'} \quad (21)$$

and τ_v is the the sum of the actual line and continuum opacities:

$$\tau_v = \tau_c + \tau_l = \tau_c + \tau_l' b_{n''} \beta_{n''n'} \quad (22)$$

In HII regions where both the line and continuum opacities are small for the radio frequency domain the actual electron temperature can be found by dividing equation (20) by the line-to-continuum ratio in LTE. This will give the actual temperature related to the LTE electron temperature as follows

$$T_e \approx T_e' \left[b_{n'} \left(1 - \frac{\beta_{n''n'} \tau_c}{2} \right) \right]^{0.87} \quad (23)$$

where T_e' is the electron temperature in LTE. In non-LTE conditions the actual line intensity depends on two competing factors, it is weakened by the depopulation of the lower level $b_{n'}$ and strengthened by the correction factor β for stimulated emission. Since $b_{n'} \leq 1$ and almost always $\beta < 0$ then the T_e' is super-thermal ($T_e' > T_e$) if τ_c is very small and sub-thermal ($T_e' < T_e$)

if $\tau_c \geq 10^{-3}$ which says that the stimulated emission is important (Brown & Lockman 1978). The departure coefficients used for determining the electron temperature in non-LTE HII regions have led to more realistic results close to that of the canonical one which is around 10^4 K. It has even been suggested rather to use the aforementioned canonical temperature and RRLs to determine the departure coefficients instead of using the latter for deriving the electron temperature (“*Radio Recombination Lines: Their Physics and Astronomical Applications*”, s. 2.3).

2.3.2 The Theory of Masering

As mentioned earlier in LTE the electronic state populations are described by the Boltzmann distribution (24) showing that there are fewer atoms in upper states than in the lower state of a transition $u \rightarrow l$.

$$\frac{N_u}{N_l} = \frac{g_u}{g_l} \exp\left(-\frac{h\nu}{kT}\right) \quad (24)$$

N_u and N_l denote here the number of atoms in upper state and in the lower state per unit volume respectively. The factors g_u and g_l are statistical weights for those states. The exponential of the equation ($\exp(-h\nu/kT) = N_l g_l / N_u g_u$) is equivalent to the one in Planck's function. In case of departure from LTE the level populations are not described by Boltzmann distribution anymore. Therefore often we may obtain population numbers differing from the ones given by equation (24). However, we can define an excitation temperature T_{ex} so that the population numbers obtained are correct when inserting T_{ex} instead of T into the equation. In LTE all the various temperatures are equal (“*Fundamental Astronomy*”, s. 5.8).

At times inverted population may occur meaning that the upper state contains more atoms per substate (i.e. N_u/g_u) than the lower state. This becomes possible by means of metastable state which has a relatively long average lifetime (Fig. 3). There the atoms are stored and accumulated until they are illuminated by photons with energies equal to the

excitation energy of the state inducing emission of photons of the same frequency. This process amplifies the radiation.

Population inversion is essential for maser emission, however, an inverted population alone will not give rise to line masering. Equation (24) shows that the excitation temperature for those cases becomes negative. When analyzing equation (11) where the electron temperature in this specific case has to be replaced by excitation temperature then we will see that the total optical depth must also become negative. Since the continuum optical depth is not be affected by population inversion the line optical depth must not only be negative but its absolute value must exceed the opacity of the continuum (*“Radio Recombination Lines: Their Physics and Astronomical Applications”*, s. 2.3; *“Tools of Radio Astronomy”*, s. 4.16).

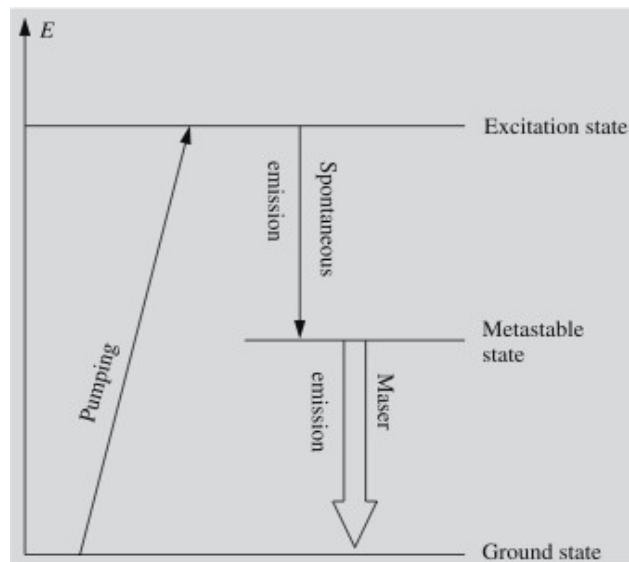


Fig. 3 The operational principle of maser. A metastable state stores atoms so that there are more atoms in metastable state than in the ground state. This population inversion is maintained by radiatively exciting atoms to a higher excitation state from which they spontaneously jump down to metastable state. When a photon with energy equivalent to the excitation energy of metastable state passes by, it will cause the atom to return to the ground state while emitting a photon of the same frequency (*“Fundamental Astronomy”*, s. 5.8).

2.4 Stellar Wind and Spectral Energy Distribution

Stellar winds play an important role in the physics of the stars and interstellar medium. The mass loss caused by stellar wind greatly influences evolution of a star. The stellar winds of hot massive stars are very strong, highly ionized and their terminal velocities can reach as high as thousands of kilometers per second. However, there exist peculiar stars with low-velocity winds (Rodriguez et al. 1982). For radiation driven winds of those hot massive stars the infrared and radio continua are produced by thermal emission from dust and free-free emission. A number of studies has been made on radio and infrared spectra of early-type stars surrounded by gaseous ionized envelope that results from mass loss. It is believed that the radiation from those objects is caused by thermal free-free emission from circumstellar ionized gas, since in many cases the excess emission detected does not seem to be due to dust emission. Measuring this continuum emission is one way to obtain information on wind properties such as ratio of mass loss rate \dot{M} and terminal velocity V_∞ . To derive the mass loss rate it is common to adopt the value for V_∞ from optical or UV observations though it is not sure that the terminal velocities of emissions of different origin coincide. The infrared thermal emission is produced in the inner part of the wind and is highly sensitive to its density structure that cannot be determined from the observations themselves. But if there are hydrogen lines arising from that region the parameters of the wind can be found. The free-free radio emission combined with radio recombination line emission produced in the outer parts of the wind will give a reliable estimation for terminal velocity of the wind and hence the mass loss rate can be derived (Rodriguez 1982; Scuderi et al. 1998).

The flux density-frequency relation for optically thin homogeneous and for optically thick homogeneous ionized isothermal gas can easily be found from equation of radiative transfer since the flux is equal to $I_\nu D^2$. For optically thin case $\tau_c \ll 1$, so the emergent intensity is of the form

$$I_\nu = B_\nu (1 - \exp(-\tau_c)) \approx B_\nu \tau_c \quad (25)$$

Using equation (10) and (12) it appears that $I_\nu \propto \nu^{-0.1}$ and thus also $F_\nu \propto \nu^{-0.1}$. For optically thick

case $\tau_c \gg 1$, hence the exponential term tends to zero in equation of radiative transfer and the intensity becomes equal to the Planck function. Using equation (12) again shows that $I_\nu \propto \nu^2$ and thus also $F_\nu \propto \nu^2$ (“*Radio Recombination Lines: Their Physics and Astronomical Applications*”, s. 2.3). Note that in case there is a strong radial gradient in density the spectral shape will be different.

On the other hand flux density-frequency relation for a stellar wind is found to be between the one expected for optically thin ($F_\nu \propto \nu^{0.1}$) and the one for optically thick homogeneous ionized gas ($F_\nu \propto \nu^2$). Several papers have derived more exact spectral energy distribution at infrared and radio continua of the form $F_\nu \propto \nu^{0.6}$ for optically thick, isothermal, uniform, spherically symmetric wind which holds for constant expansion velocity (Wright & Barlow 1975; Panagia & Felli 1975). In the following the summary of the derivation of the latter will be shown. The gas number density changes as $n(r) \propto r^{-2}$. Consider a mass flow from the surface of central star originating at radius R_c where the ionized gas is ejected at a uniform rate with constant velocity V_∞ . The mass loss rate can be given by

$$\dot{M} = 4\pi r^2 n \mu m_H V_\infty \quad (26)$$

where r is the radial distance from the center of the star, μ is the mean atomic weight of the gas and m_H is the mass of hydrogen atom. Solving the equation for gas number density gives us

$$n = \frac{\dot{M}}{4\pi \mu m_H V_\infty r^2} \quad (27)$$

The geometry of the model is shown in figure 4. We depict a thin cylindrical shell of the out-flowing gas with a projected radius q . By solving the equation of radiative transfer in LTE approximation we get the intensity of emergent radiation from this thin shell as

$$I_\nu = B_\nu (1 - \exp(-\tau(q))) \quad (28)$$

where $\tau(q)$ is the total optical depth along the cylindrical shell at the distance of projected radius q which can be found by integrating the gas number density over the path length l through the nebula.

$$\tau(q \geq R_c) = \kappa(\nu) \int_{-\infty}^{\infty} n^2 dl = \frac{\pi}{2} \frac{\kappa(\nu)}{q^3} \left[\frac{\dot{M}}{4\pi \mu m_H V_\infty} \right]^2 \quad (29)$$

We do not consider $\tau(q < R_c)$ since for high enough mass loss rate or low enough frequency the flux density at those conditions tends to zero and its contribution is negligible. Here $\kappa(\nu)$ is the linear free-free absorption coefficient that for the radio range is given in cgs units by Panagia & Felli (1975) as:

$$\kappa(\nu, T_e) = 8.436 \cdot 10^{-28} \left(\frac{T_e}{10^4 K} \right)^{-1.35} \left(\frac{\nu}{10 \text{ GHz}} \right)^{-2.1} \quad (30)$$

The flux density received from the thin shell by the observer from distance D is

$$dF_\nu = \frac{B(\nu)}{D^2} [1 - \exp(-\tau(q))] 2\pi q dq \quad (31)$$

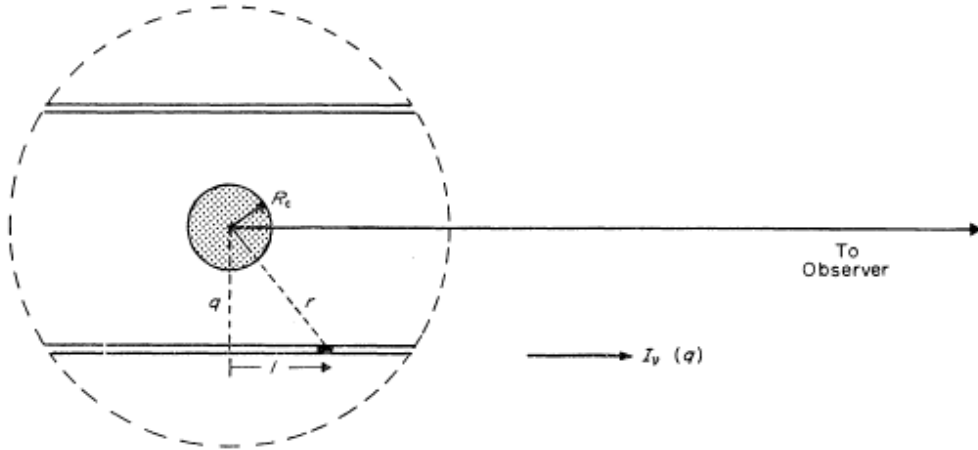


Fig. 4 Geometry of the model of an ionized, uniform, spherically symmetric mass flow with constant expansion velocity (Wright & Barlow 1975)

To obtain the total flux density, equation (31) must be integrated along the line of sight over the

entire structure. That gives the total flux density in cgs units as

$$F_\nu = 1.33 \cdot 2 \pi \cdot \left(\frac{\pi}{2}\right)^{2/3} \left(\frac{\dot{M}}{4 \pi \mu m_H V_\infty}\right)^{4/3} \frac{1}{D^2} \cdot B(\nu, T_e) \kappa^{2/3}(\nu, T_e) \quad (32)$$

This in turn can be written for the radio and infrared regions of the spectrum where $kT \gg h\nu$ in units of mJy as given by (Scuderi et al. 1998)

$$F_\nu = 7.26 \left[\frac{\nu}{10 \text{ GHz}}\right]^{0.6} \left[\frac{T_e}{10^4 \text{ K}}\right]^{0.1} \left[\frac{\dot{M}}{10^{-6} M_\odot \text{ yr}^{-1}}\right]^{4/3} \left[\frac{\mu V_\infty}{100 \text{ km s}^{-1}}\right]^{-4/3} \left[\frac{D}{\text{kpc}}\right]^{-2} \quad (33)$$

The dependence of the emission on the electron temperature is rather weak here and since the relevant emitting region for every frequency is relatively narrow, it indicates that the temperature gradients are not playing a remarkably role. With that we have flux density for free-free emission that varies as $F_\nu \propto \nu^{0.6}$.

We can find the effective radius $R(\nu)$ for the emitting region at each frequency so that the flux density given by equation (33) is equivalent to the one arising exterior to this radial distance. It is defined by radial optical depth of $\tau_\nu = 0.244$. Now the effective radius can be estimated by combining equations (29) and (33). We find that the characteristic radius of the emitting region in units of cm is given by

$$R(\nu) = 2.8 \cdot 10^{28} g^{1/3} T_e^{-1/2} \left[\frac{\dot{M}}{\mu V_\infty \nu}\right]^{2/3} \quad (34)$$

where g is the Gaunt factor. Since for uniform flow the electron density $n(r)$ varies as shown in equation (27) we can estimate the expected electron density using the estimate of the effective radius.

Spectral energy distribution for Eta Carinae and Homunculus nebula from near infrared to radio wavelengths given in figure 5. Gomez et al. (2010) shows the SED with featured variability of the flux due to the radio cycle of 5.5 years. There are three major components of SED: thermal emission from dust peaking at about 20 μm , varying free-free emission from the ionized wind and an optically thin free-free emission tracing the extended ionized gas

associated with the Little Homunculus. The latter is believed to be produced by the ionization of the wind of Eta Carinae by UV radiation from a possible hot binary companion (Gomez et al. 2010). The SED of the ionized wind is divided into two components: optically thin wind varying as $F_\nu \propto \nu^{1.3}$ which puts the spectrum somewhere between the classical spectra of ultra compact HII regions ($F_\nu \propto \nu^2$) and the second component, optically thick stellar wind varying as $F_\nu \propto \nu^{0.6}$. Cox et al. (1995b) suggests that there is a transition between those two power-law regimes where the flux density flattens to $F_\nu \propto \nu^1$. It is argued that the deviation from the flux density expected for a fully ionized stellar wind can be explained by non-uniform mass loss rate, or by changes in the ionization structure. If hydrogen starts to recombine in the outer regions of the wind, the the fraction of the neutral gas increases changing the ionization structure and causing the spectrum to steepen. Assuming changes in the ionization structure the gas number density was estimated to change as $n(r) \propto r^{-3.5}$. The gas number density at 230 GHz (spectral index =1.3) was derived to be $\sim 10^7 \text{ cm}^{-3}$ at electron temperatures $T_e = 10^4 \text{ K}$.

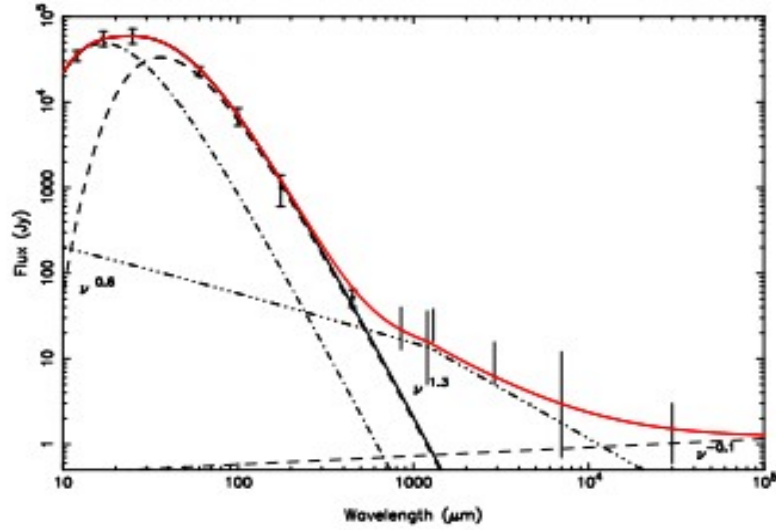


Fig. 5 The spectral energy distribution (SED) of Eta Carinae from near infrared to radio wavelengths. Vertical bars indicate the variability range of the radio and mm wavelength cycle during 5.5 years. The solid black line represents the sum of two temperature modified black-bodies (174 K and 82 K) and 450 μm (dot-dashed and dashed respectively). The dot-dot-dot-dashed line shows the SED expected from the optically thick free-free wind with flux density $F_\nu \propto \nu^{0.6}$ and optically thin wind with $F_\nu \propto \nu^{1.3}$. The dashed line represents emission from the optically thin Little Homunculus feature $F_\nu \propto \nu^{0.1}$. The red line shows the total SED from all the components (Gomez et al. 2010).

The continuum fluxes observed in August and November 1991 for 231 GHz and 99 GHz were found to be 24.1 Jy and 9.2 Jy respectively (Cox et al. 1995b). Taking into consideration the 5.5 year radio cycle we would expect the phase of this cycle in 1991 and the phase of the cycle of current observation to coincide. Therefore in LTE conditions we would expect the continuum fluxes for mentioned frequencies to agree in the two phases.

2.5 Line Broadening by the Stark Effect

Among other broadening effect the Stark effect is at times most important mechanism for RRLs. Stark effect appears in spectral lines when the line-emitting source is exposed to an external electric field causing the spectral lines to split into several components. In other words when a freely moving electrons or ions come close to an excited atom it will “feel” their electrical charges that will change the atomic energy levels of this excited atom by splitting and displacing them. As a result an electron cascading down to lower energy levels will have to cover an energy change ΔE that is different compared to an unaffected atom (Fig 6). Therefore also the photon radiated will have a frequency different from the one emitted by an unaffected atom (*“The Astrophysics of Emission-Line Stars”*, s. 2.6).

The electric field “felt” by this emitting atom is usually not a steady-state field but might consist of a series of brief, weak and time-spaced transient fields induced by a series of successive colliding charged particles. These transitory encounters are called collisions or impacts.

This effect is classified into two cases: Linear Stark effect and quadratic Stark effect. The linear type occurs for weak electric fields and is seen in hydrogen and hydrogen-like atoms. The conditions in interstellar plasmas and stellar atmospheres vary widely and therefore no unified theory of Stark effect can be used but an appropriate approximation must be selected. It has become clear that for most of HII regions impact approximation (discrete, separated impacts) which is dominated by collisions with electrons is appropriate for calculating Stark broadening for RRLs. This impact broadening can be either elastic or inelastic. Elastic collisions do not result in exchange of energy. The interaction splits and shifts the energy levels but does not change the n value. Inelastic collisions on the other hand do that

in addition to the splitting and shifting. Conventionally both elastic and inelastic type of collisions of excited atoms with electrons can occur for RRLs in HII regions. For ion-atom collisions only elastic collisions can occur (“*Radio Recombination Lines: Their Physics and Astronomical Applications*”, s. 2.2).

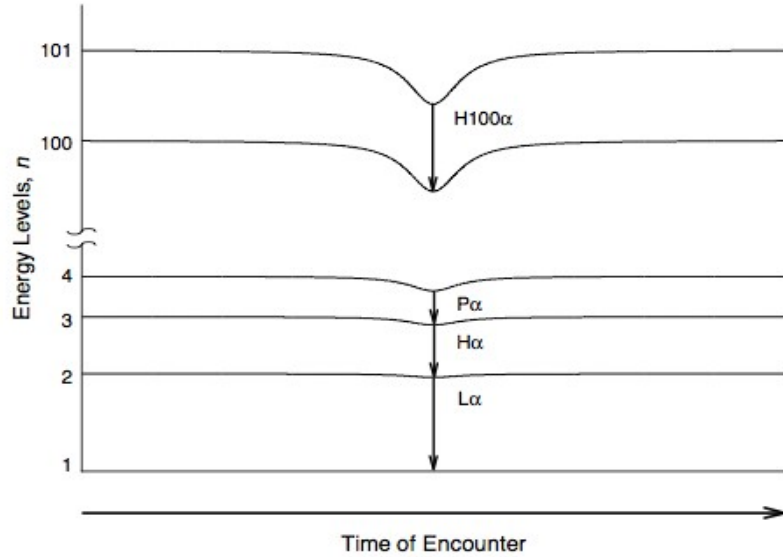


Fig. 6 Distortion in the energy of Stark components of quantum level n caused by elastic collisions. Unlike the optical lines (the first three), similar distortions of high- n levels compensate for each other to reduce the Stark broadening of RRLs (Gordon, M.A.)

It is commonly accepted that the majority of the broadening of the radio recombination lines of high- n values with Stark broadening is due to the contribution of inelastic collisions with electrons (Fig 7). The formula for estimating the width (half width at half maximum) due to this pressure broadening for RRLs has been given by

$$\Delta \nu_L^e = 8.2 \cdot n(e) \left(\frac{n}{100} \right)^\gamma \left[1 + \frac{\gamma \Delta n}{2n} \right] \quad (35)$$

where the average value for γ , that is a weakly changing function of temperature, is 4.5. In most of the studies this broadening has been observed in much higher atomic energy level than in

present case (Smirnov 1984 ; De Pree et al. 2004; Oks 2004).

Another look at figure 7 shows that for decreasing quantum numbers the elastic ion collisions is starting to play an important role. The expression for the elastic ion collision width is

$$\Delta \nu_L^i = \frac{6.7 \cdot 10^{-6}}{\sqrt{T_e}} n(i) n^2 \ln(172n) [\ln(9.4 \cdot 10^{-3} n^2 \sqrt{T_e})] \quad (36)$$

where the ion number density n_i for simplicity can be taken to be equal to electron number density n_e . The total line width caused by pressure broadening is the sum of equation (35) and (36). The result is in units of Hz but can easily be converted into units of km/s using the relation $\Delta V = \Delta \nu c / \nu$.

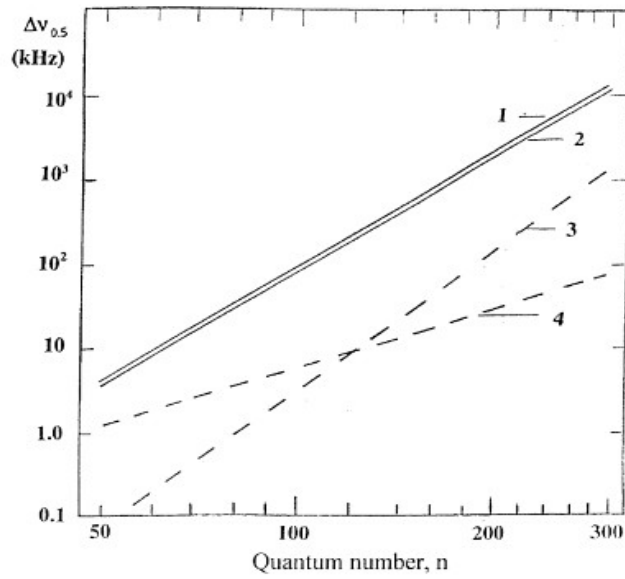


Fig. 7 Stark broadening of hydrogen RRL in plasmas as a function of quantum number n for electron density and ion density $n_e = n_i = 10^4 \text{ cm}^{-3}$ and electron temperature $T_e = 10^4 \text{ K}$. Line 1 and 2 show the broadening by inelastic electron collisions, the difference being the approach. Line 3 shows inelastic ion collisions and line 4 elastic ion collisions (“*Radio Recombination Lines: Their Physics and Astronomical Applications*”, s. 2.2).

Usually RRLs have line profiles that are influenced both by thermal effects and linear Stark effects. These two give a Gaussian profile and Lorentzian profile respectively. Convolution of those two will result in Voigt profile which is very common for emission lines.

2.6 Maser Emission Detection in Millimeter Recombination Lines Towards Eta Carinae

A set of hydrogen recombination lines from Eta Carinae was observed and analyzed by Cox et al. (1995a). The H30 α , H29 α and H37 β recombination lines were detected with a wide central peak (~ 40 km/s) with an intensity of about 1 K on top of a very broad emission plateau (-200 km/s - 100 km/s) with an intensity of about 0.1 K. The coverage of that broad range for the underlying plateau is very rare for recombination lines. The profile shape of the underlying plateau was found to be asymmetrical with enhanced blue-shifted emission that is also remarkable. The ratios of β/α lines studied were significantly smaller than expected from LTE emission which led to consideration of stimulated emission affecting the α lines.

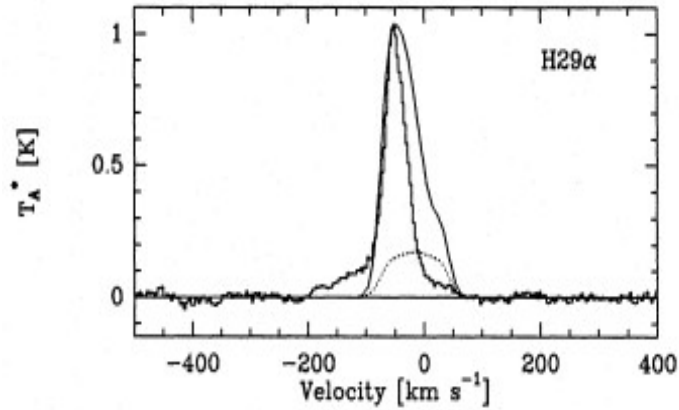


Fig. 8 Model predictions of H29 α line profile emitted in LTE (dashed line) and in non-LTE (smooth solid line) conditions superimposed on the observed spectra. Isothermal ionized stellar wind (~ 15000 K) with density structure $r^{-3.5}$ and constant expansion velocity of 58 km/s is considered for the model (Cox et al 1995a).

One can see on figure 2 that for smaller n values the stimulated emission coefficient becomes negative at higher densities than for larger n values. One must determine at what densities and temperatures the stimulated emission coefficient is negative for a certain frequency. It is shown in Walmsley (1990) that for current frequencies (n values) the stimulated emission coefficient becomes negative at relatively high densities ($\sim 10^7 \text{ cm}^{-3}$) for electron temperatures $T_e = 10^4 \text{ K}$. This gives a reason to believe that the maser emission is present since the gas number density derived from millimeter continuum emission mentioned earlier is perfectly in agreement with the latter. A constraint to the maser region size and the transparency of the core around the central star is put by density distribution $n(r) \propto r^{-3.5}$. In other words the maser region is small and the core is highly optically thick blocking the radiation coming from behind and this way affecting the intensities and profile shapes of the recombination lines. We will look more deeply into one of the recombination lines

The results of a model calculation for continuum and recombination lines in LTE and non-LTE conditions is shown on the figure 8 superimposed on the observation spectra for H29 α . The dashed line shows the expected intensity and profile shape of the line emitted under LTE conditions. Due to opacity of the continuum it is much weaker than would be expected from optically thin case. One can see that its peak does not coincide with the one observed. In addition the electron temperature estimated from the observed intensities are very low indicating that LTE condition can be ruled out. The smooth solid line represents the non-LTE results. Since only the ionized gas in front of the optically thick core would be affected by stimulated emission the recombination line would undergo a blue-shifted enhancement that can also be seen in observations. The modeled non-LTE line intensity and shape is in a good agreement with the measurements. The deviations could be explained by the complex gas distribution around Eta Carina which can not be perfectly describe by simple geometry, distribution of matter and velocity field.

A similar outcome was announced by Abraham et al. (2002) where the H30 α , H35 α and H40 α recombination lines were studied in comparison to the observed underlying continuum during the time the continuum flux density was at its maximum. By constructing a simplified model of the emitting region and solving the equation of radiative transfer under non-LTE conditions they arrived to a rather good agreement between the model and observational profile while the applied LTE conditions again gave a completely differing result.

It might be useful in terms of later analysis to mention here that the temperature fitting

the observed line profile was found to be $T = 8800$ K with the line peaking at -56 km/s and turbulent velocity (20 km/s) was considered to account for the broadening of the line. Both of the studies however describe the disk emission with differential motion not emission due to free-free wind described by a spherical model above.

3. WORKING WITH DATA

3.1 The Observations

The observations of the H I 26 α line were made at the Atacama Pathfinder EXperiment (APEX) telescope, Cerro Chajnantor, Chile, on 2008 October 22 and December 21. The program identification number is O-082.F-9316A. The conditions were good on both dates, with a system noise temperature in the range 400 to 440 K at 353.6 GHz. The facility heterodyne receiver was used together with a spectrometer configuration that yielded a resolution of 244.1 kHz or 0.207 km/s in Doppler velocity. A total of 44 minutes integration time was used.

3.2 Data Analysis

3.2.1 Fitting the Line Profile and Comparing It to the Results Obtained from Simple Wind Model in LTE

In current project MatLab has been used to analyze the data. The first step was to remove the underlying continuum emission. Usually it can be taken to be a linear function, but since in this specific case the response of the receiver is slightly non-linear across the bandpass, a polynomial had to be fitted to get more precise results. The best fit for continuum turned out to be a fifth order polynomial which is rather high but the lowest order polynomial that gives a satisfying outcome.

Assuming the line profiles to be Gaussian a Gaussian fit was applied by using Curve Fitting Tool in MatLab. The best fit was obtained by decomposing the H26 α line profile into seven Gaussians of different widths while one Gaussian presented the He26 α line profile. One fit covered both the emission lines. When the He26 α line was neglected the H26 α line could be fitted with three Gaussians of different width (Fig. 9).

Figure 9 visualizes the fit overlying the data. The prominent blue shifted peak corresponds to H 26α line at frequency 353.688 GHz and the even more blue shifted small bump to the left of it is the result of He 26α emission at frequency 353.834 GHz. The best fit for both line profiles is denoted with the blue line and the hydrogen line profile is shown with the red line. It is evident that the difference between two fits is not remarkable therefore the simpler fit of three Gaussians will be used for further analysis.

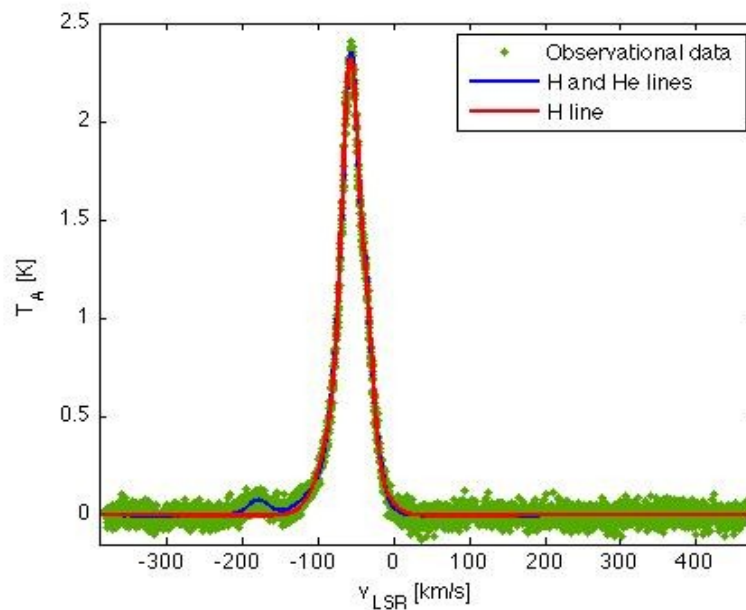


Fig. 9 The vertical axis presents the intensity as antenna temperature in K and the horizontal axis is the Doppler radial velocity in the Local Standard of Rest (LSR) reference frame in km/s. The red line presents the fitted curve for H line only using 3 Gaussians of different widths. The blue line presents the fitted curve of both H and He lines using 8 Gaussians of different widths.

Figure 10 shows the observed hydrogen line profile decomposed into three Gaussians. The smallest peaked component is strongly deviated from the expected line center. This feature causes the strong enhancement in the right wing that can be seen as a bump in the observed line profile (black line). It could be caused by radiation arising from a different region and only appears to be part of the region in question by the effect of line blending (Ignace 2009). This

however is merely an assumption. Both of the H line profile wings show broadening effect. It is possible that this is due to collisional broadening which will later be looked into in more detail. Apparently the wings look asymmetrical with a rather strong but smooth broadening in the left wing.

The values of interest were obtained by using the analyzing option for the fitted curve. The line peak intensity of H26 α was found to be 2.32 K while the underlying continuum intensity was 0.89 K. For He26 α line the peak intensity was 0.08 K while the underlying continuum emission was 0.87 K. These intensities are given in antenna temperature in table 1. The observations were carried out with the receiver APEX-2a which has Kelvin to Jansky conversion factor of 41, hence the antenna temperatures can easily be converted into Janskys (Güsten et al. 2006).

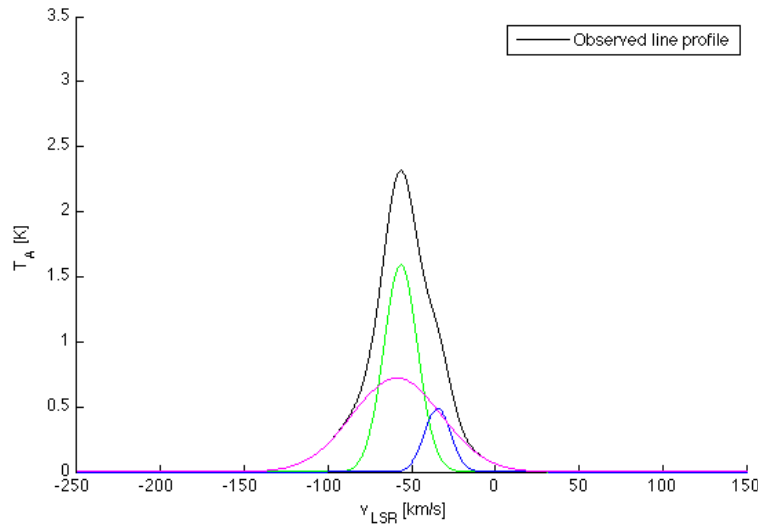


Fig. 10 Decomposition of the observed hydrogen line profile into three Gaussians of different width.

Assuming that the relative abundance of He and H is constant throughout the nebula where helium is singly ionized (Dupree & Goldberg 1970). Note that equation (37) expects both helium and hydrogen to be ionized to the same extent. The integrated intensities given in Table 1. show that the relative abundance in the present case is much lower – $N(\text{He})/N(\text{H}) = 0.028$. This discrepancy could be the result of the amplification of hydrogen line by masering to a

greater extent than the helium line or simply because helium is less ionized than hydrogen.

Table 1. Line peak intensities and integrated intensities in antenna temperature from the observations

	Peak intensity	Integrated	Continuum
	[K]	intensity [K km/s]	intensity [K]
<i>H26α</i>	2.32	98.9	0.89
<i>He26α</i>	0.08	2.8	0.87

It yields from the fitted line profile that the line peaks at -56.4 km/s and the line width at half maximum is 36.3 km/s. The line-to-continuum ratio of hydrogen line obtained from the values in Table 1. and the line can be used to estimate the electron temperature using equation (16). With the above estimated relative abundance of He and H we find it to be $T_e \approx 11000$ K. Electron temperature for HII regions in LTE generally have the value of about 10^4 K so the obtained result lies close to the canonical value. According to this result one can expect the gas to be in LTE and the emission to be quasi-thermal but very intense.

Let us now take a similar approach to the one used in Cox et al. (1995a) in order to find out what we would expect the recombination line profile to look like in LTE conditions. To find the relevant parameters a pre-coded Fortran program (by John Black) was used. It is a model calculation described in section 2.4 that computes the spectrum of a steady, homogeneous ionized stellar wind of a hot star with H lines in LTE. There are four free parameters in this stellar wind model: mass loss rate, electron temperature, terminal velocity and distance to the object. The mass loss rate is estimated from equation (33) and its value $\dot{M} = 3.15 \cdot 10^{-3} M_{\odot}/\text{yr}$ corresponds to the previously obtained electron temperature of 11000 K. The distance to the object $D=2.35$ kpc is adopted from preceding studies. Massive early-type stars are known to have winds of very high terminal velocity sometimes up to thousands of kilometers per second. We assume here a moderately large terminal velocity of $V_{\infty}=500$ km/s for Eta Carinae's wind as suggested by Smith et al. (2003a). The continuum flux density for the wind model with mentioned parameters is 36.6 Jy. The corresponding line flux is $5.364 \cdot 10^{-14}$ erg/cm²/s which gives the line-to-continuum ratio roughly of the order of one smaller than the one from observations. This corresponds to the line width which is taken to be equal to terminal velocity in the LTE wind model. On figure 11 one can see the comparison of two line profiles which

shows that this kind of high terminal velocity of the wind would be ruled out in case the emission line really is formed in the wind region. The results are summarized in Table 2.

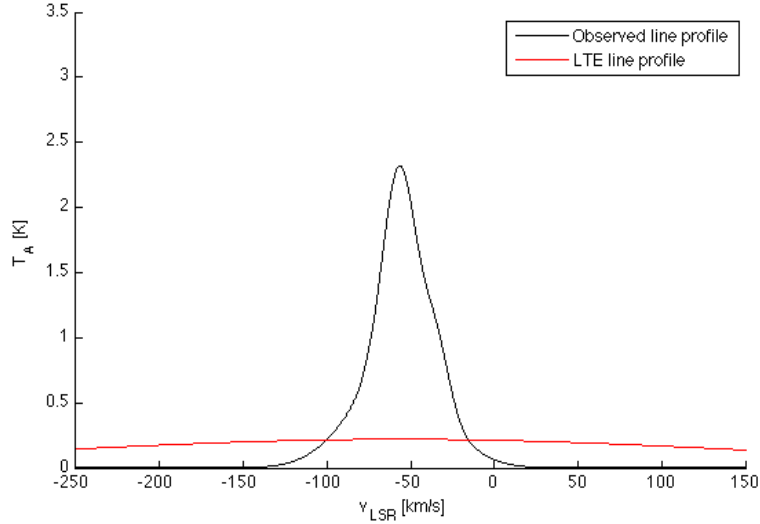


Fig. 11 Comparison of the observed line profile to the line profile from LTE wind model with $T_e=11000$ K and $V_\infty=500$ km/s.

Table 2. Line and continuum flux densities of the observed line profile and the LTE wind model at temperature $T_e=11000$ K and terminal velocity $V_\infty=500$ km/s.

	Continuum flux [Jy]	Line flux [erg/cm ² /s]	Line-to-continuum ratio	Line width [km/s]	Peak center [km/s]
Observed	36.5	$4.07 \cdot 10^{-14}$	2.606	36.3	-56.4
LTE model	36.6	$5.36 \cdot 10^{-14}$	0.248	500	-56.4

The previous approach is simplified to a great extent using robust assumptions and without considering some important factors that can change the results significantly. As we see the outcome is not very satisfying either. Hence it is useful to redetermine the necessary parameters with more precision while still keeping the model fairly simple.

As already mentioned the environment of Eta Carina is very peculiar with its high IR

emission. The SED in figure 5 shows that thermal emission from dust can contribute remarkably to the continuum emission up to millimeter wavelengths. The estimated contribution for frequency 353 GHz from that SED can vary from about 10% up to 20% depending on the phase of the radio cycle. Since the phase of the radio cycle of present observations lies roughly at half maximum, the estimated contribution by thermal emission from dust is approximately 15%. This reduces the observed continuum flux density from free-free emission to ≈ 31 Jy. Estimating the electron temperature from equation (16) again results in $T_e \approx 9800$ K. As one realizes this does not affect the line profile and hence the line flux density of the observed profile remains the same. It yields from the observations that the line profile is very narrow and therefore we would expect the velocity of the wind to be quite small. With mass loss rate of $\dot{M} = 2.05 \cdot 10^{-4} M_{\odot}/\text{yr}$ we get the continuum flux density of 31.1 Jy and line flux density of $5.27 \cdot 10^{-14}$ erg/cm²/s at terminal velocity equal to the observed line width. The line-to-continuum ratio of 3.958 is about one third larger than the one from observations. The summary of the results are presented in Table 3.

Table 3. Line and continuum flux densities of the observed line profile and the LTE wind model at temperature $T_e=9800$ K and terminal velocity $V_{\infty}=36.3$ km/s.

	Continuum flux [Jy]	Line flux [erg/cm²/s]	Line-to-continuum ratio	Line width [km/s]	Peak center [km/s]
Observed	31	$4.07 \cdot 10^{-14}$	3.068	36.3	-56.4
LTE model	31.1	$5.27 \cdot 10^{-14}$	3.958	36.3	-56.4

We want to check now if the line profiles obtained in two different methods will show similarities or is the deviation so remarkable that the non-LTE approach should be applied instead. For this purpose the relevant parameters obtained from LTE model are used to represent them graphically as a line profile that we compare with the line profile obtained from the observations. The LTE line profile is assumed to be a simple Gaussian.

On figure 12 we can see that the profile expected for LTE conditions is showing a larger peak intensity than the observed one. Hence the implication of LTE would not be incorrect and with that the maser emission would be ruled out. The line profiles appear to be somewhat similar with the integrated intensity of the LTE line profile being 25% larger than the

integrated intensity of the observed line.

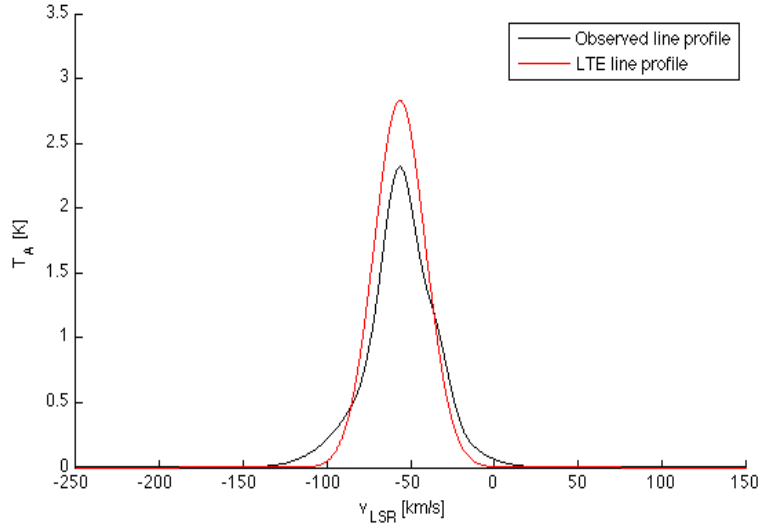


Fig. 12 Comparison of the observed line profile to the line profile from LTE wind model with $T_e=9800$ K and $V_\infty=36.3$ km/s.

It has become clear that stellar winds are not laminar or “smooth” but rather “clumpy”. The clumping can play an essential role in affecting the mass loss rate derived from radio emission. This happens because the received flux density is dependent on free-free opacity which in turn scales with the square of the wind density and clumping introduces a variability in density (Ignace 2009). For simplicity we assume the wind to have a constant clumping factor. In this case the terminal velocity can be found from the equation

$$\frac{\Delta V}{2} = 0.87 V_\infty \quad (38)$$

when the lines are emitted in optically thin wind. The best estimate we can get for terminal velocity is to use the observed line width in equation (38) which yields $V_\infty=20.9$ km/s. It must be mentioned though that such a result for wind velocity is surprisingly small for a massive star like Eta Carinae. With the change in terminal velocity and hence in line width the estimate of electron temperature becomes $T_e \approx 15900$ K. Such an estimate of temperature is a good one for

stellar wind distant from the surface of the central star. The best estimate for mass loss rate is $\dot{M} = 1.11 \cdot 10^{-4} M_{\odot}/\text{yr}$. The LTE wind model with those parameters gives us the continuum flux density of 31 Jy and the line flux density of $2.85 \cdot 10^{-14} \text{ erg/cm}^2/\text{s}$. The line-to-continuum ratio is slightly decreased if we compare it to the previous case. The results are summarized in Table 4.

Table 4. Line and continuum flux densities of the observed line profile and the LTE wind model at temperature $T_e=15900 \text{ K}$ and terminal velocity $V_{\infty}=20.9 \text{ km/s}$.

	Continuum flux [Jy]	Line flux [erg/cm ² /s]	Line-to-continuum ratio	Line width [km/s]	Peak center [km/s]
Observed	31	$4.07 \cdot 10^{-14}$	3.068	36.3	-56.4
LTE model	31	$5.26 \cdot 10^{-14}$	3.744	20.9	-56.4

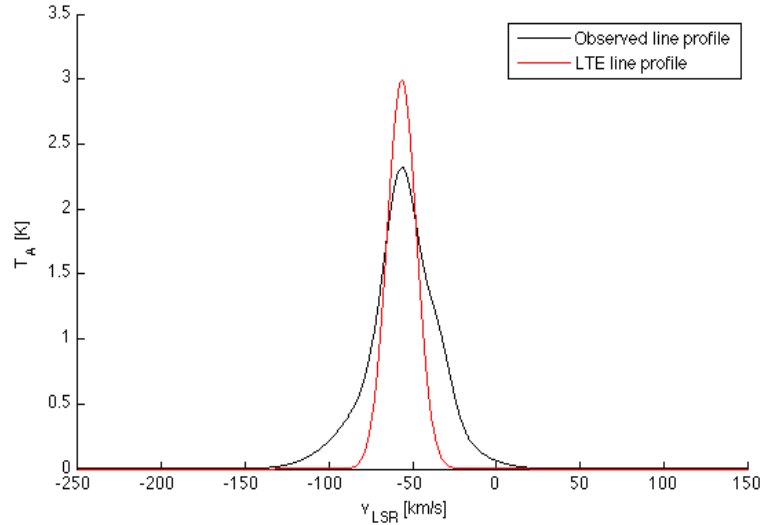


Fig. 13 Comparison of the observed line profile to the line profile from LTE wind model with $T_e=15900 \text{ K}$ and $V_{\infty}=20.9 \text{ km/s}$.

Figure 13 reveals that the line peak intensity has decreased slightly if compared to the previous one. Clearly the width of the LTE line is very narrow and therefore the profiles do not coincide as well as in previous case. The integrated intensity of the observed line profile is 56%

larger than the one from LTE line profile. This would mean that unless the net power in this line comes from different regions the emission is stronger than expected in LTE conditions which could refer to stimulated emission.

3.2.2 LTE Line Profile with Broadening Effect

As mentioned earlier the line broadening may be a result of pressure broadening also called as Stark effect. To find out how the effect affects the shape of the line we need to give an estimate to electron number density. First we use the simple case of constant electron density and static nebula to . The intensity of the emission can be found from

$$I_{\nu} = \frac{F_{\nu}}{\Omega_b} \quad (39)$$

where F_{ν} is the flux density of the continuum and Ω_b is the beam area. The latter can be found by using main beam width θ_{mb} in equation $\Omega_b = \pi(\theta_b/2)^2$. The main beam width for the receiver APEX-2a at frequency 352 GHz is 17.3" (Güsten et al. 2006). Combining the result with equation (9) while assuming an optically thin medium we will have

$$B_{\nu}(T_e)\tau_c = 6.6 \cdot 10^{(-14)} \quad [cgs] \quad (40)$$

Inserting equation (12) for continuum opacity will allow us to find the emission measure of continuum which in present case is $E_c = 1.2 \cdot 10^8 \text{ cm}^{-6} \text{ pc}$. This corresponds to the average emission measure over the area of the projected beam. In practice, if the emitting region is smaller than the projected beam, the emission measure obtained will be smaller than the actual emission measure due to the attribution of some fraction of it to the non-emitting region. From figure 1 we can see that the emitting region does not cover the the whole area of the projected beam hence we can expect the actual emission measure to be somewhat larger than previously estimated. The estimated filling factor could be somewhere around 1/10. For constant electron density the emission measure can be written $E_c = n_e^2 L$ where the path length L through the

emitting region is here taken to be the one for projected beam and hence can be estimated from the main beam width θ_{mb} and the distance D to the object. For small enough angles $L=\theta_{mb}\cdot D$. The estimation of emission measure and the path length for the projected beam allow us to estimate the electron number density of the emitting region which approaches $n_e=2.47\cdot 10^4\text{ cm}^{-3}$.

In case of uniform flow the electron number density is varying as shown in equation (27). For the radius we adopt the effective radius found from equation (34) which in present case at electron temperature $T_e=9800\text{ K}$ is $R(\nu)=2.18\cdot 10^{15}\text{ cm}$. The obtained electron number density is $2.82\cdot 10^7\text{ cm}^{-3}$. Now it is easy to estimate the line width caused by Stark effect. Using equations (35) and (36) the estimated broadening resulting from this effect is 1.1 km/s . The left panel of figure 14 shows that the resulting Voigt profile lies close to the LTE profile rather than to the observed profile. Its integrated intensity is $\sim 17\%$ larger than from the observed profile. The right panel visualizes the Voigt profile with Stark broadening component with the width increased by factor of 5. One can see a rather good consistency between the observed profile and Voigt profile. However increase in width of pressure broadening results also in the increase of electron number density by factor of 5.

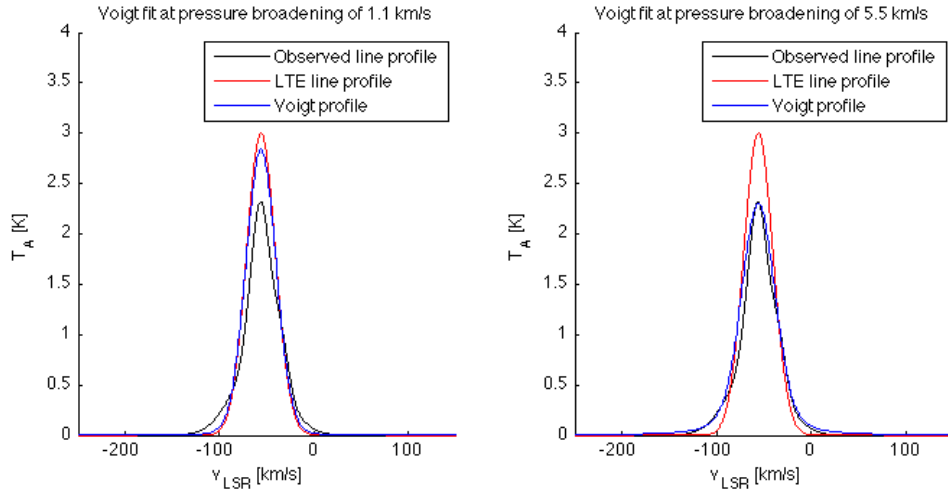


Fig. 14 Voigt function for the line with $T_e=9800\text{ K}$ and $V_\infty=36.3\text{ km/s}$. *Left*: obtained from convolution of LTE profile with pressure broadening of width 1.1 km/s . *Right*: obtained from convolution of LTE profile with pressure broadening of width 5.5 km/s .

For temperature 15900K and terminal velocity 20.9 km/s we find the effective radius to be $1.71 \cdot 10^{15}$ cm and with it the estimate of electron number density is $4.32 \cdot 10^7$ cm^{-3} . This yields the width by pressure broadening to be 1.5 km/s. One can see on figure 15 no consistency between the observed profile and the Voigt profile. Changing the width of pressure broadening will not lead to any better results either but instead shows a shrinking peak intensity compared to the one observed with its integrated intensity being only 62% of the latter.

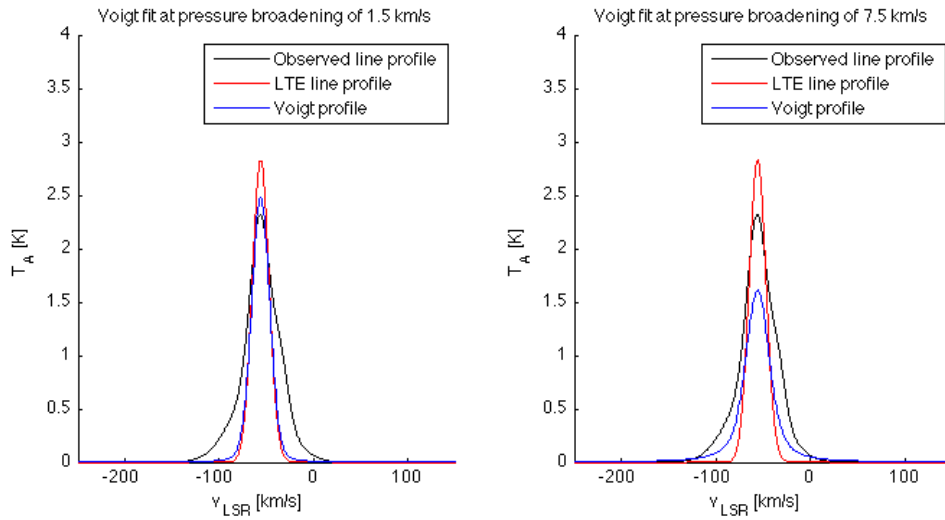


Fig. 15 Voigt function for the line with $T_e=15900$ K and $V_\infty=20.9$ km/s. *Left*: obtained from convolution of LTE profile with pressure broadening of width 1.5 km/s. *Right*: obtained from convolution of LTE profile with pressure broadening of width 7.5 km/s.

For the model with $T_e=9800$ K and $V_\infty=36.3$ km/s the Voigt profile fit shows a fairly good result even though the electron number density needs to be slightly larger than expected from the LTE model. Since the actual source is complex this discrepancy could be attributed to the simple model of uniform flow. Moreover the assumption of the observable line width being comparable to the terminal velocity is a notable simplification to the radiative transfer. The line broadening theory used here was originally derived for high n-levels and might change its scaling for smaller quantum numbers like the one in question.

3.2.3 Changes in the Line Intensities

The subsequent observation have shown very abrupt changes in the line flux density of H29 α line over a period of only about three months (private communication with Rodrigo Parra). The time variability can be distinguished into two cases: variation of the mass loss rate and variation of the ionization.

The variation in mass loss rate usually do not show that short variability in radio recombination lines even if the variation in mass loss rate is instantaneous. It can be of the order of weeks or months. The possibility to observe this variation depends on the timescale of the intrinsic variation and hence if it occurs over a time shorter than a few weeks the variation will completely be averaged out in the radio. The time for transit can be estimated in hours as shown in Scuderi et al. (1998)

$$t_{transit} = \frac{R_{eff}}{V_{\infty}} = 19.3 \left[\frac{R_{eff}}{10R_{\odot}} \right] \left[\frac{V_{\infty}}{100 \text{ km/s}} \right]^{-1} \quad (41)$$

For a low-velocity wind of terminal velocity of $V_{\infty}=36.3$ km/s this results in 25 years and even longer time for $V_{\infty}=20.9$ km/s. It is obviously too long time to be responsible for the changes observed.

Since the changes observed happened during the predicted binary eclipse it could be explained by the binary companion shadowing the region where the line emission arises from the ionizing radiation (Smith et al. 2003a). However for that to happen the recombination time

t_{rec} must be shorter than the time-scale of variation, that is $t_{rec} \leq 1$ month. The recombination time in seconds case can be estimated from equation given by Scuderi et al. (1998) again

$$t_{rec} = 7.4 \left[\frac{\dot{M}}{10^{-6} M_{\odot} / yr} \right]^{-1} \left[\frac{R_{eff}}{10R_{\odot}} \right]^2 \left[\frac{V_{\infty}}{100 \text{ km/s}} \right] \left[\frac{\mu}{1.3} \right] \left[\frac{T}{10^4 \text{ K}} \right]^{0.8} \quad (42)$$

For constant density and static nebula the recombination time with the corresponding electron number density would be about 5 years which is definitely too long time for current changes. The electron number density and hence the mass loss rate estimated for the uniform flow of temperature $T_e=9800$ K is considerably larger and results in recombination time of roughly 34 hours. Similar result is obtained for temperature $T_e=15900$ K. Large changes in photo-ionization rate in a dense nebula could explain the variation. However, this would require that the shadow-zone due to the eclipse must cover a large fraction of the nebula volume. This could work for a thin disk but not for a uniform, spherical nebula.

4. CONCLUSIONS

The electron temperature obtained by using the simplified model with local thermodynamic equilibrium conditions turned out to be rather close to the canonical temperature of HII regions. Two different cases were discussed: model with $T_e=9800$ K and $V_\infty=36.3$ km/s and another model with $T_e=15900$ K and $V_\infty=20.9$ km/s. Both of the modeled profiles are rather similar in terms of line peak intensities giving a reason to believe that the emitting region is under LTE conditions. On the other hand in the second case the integrated intensity of the observed profile is considerably larger than the one from wind model. The first one shows a rather good consistency to the observed line profile when impact broadening was applied to it and the electron number density assumed to be of the factor of 5 larger than expected from the wind model. The second case did not produce any satisfying results even after modifying the conditions. We can not be completely sure that comparing the observed line width to terminal velocity is suitable even though it gives a nicely fitting result. Hence the misfit in the second case could result from the fact that terminal velocity estimation for this case, following the arguments by Ignace (2009), is not the best one.

If we consider the first case to be correct there still remains the difference in estimated electron number density and the one we would expect according to the fitting Voigt profile. This could be explained by density distribution deviation from steady flow. When trying to compare the recombination time from recently observed changes in line intensity and the one expected from the wind model we see a remarkable difference with the expected wind model showing a considerably shorter recombination time.

All in all since the actual velocity field and the gas number density variability as well as the structure of the studied object is more complex than the one described by the model calculus with numerous approximations, the resulting LTE estimation may deviate from the actual conditions. Unfortunately there is no straightforward model yet that would describe the physical conditions of Eta Carinae's surroundings.

It still remains a question whether the emission originates from low-velocity wind or ionized nebula. Perhaps the best solution will come from future observations with ALMA, which will resolve the internal structure of the Homunculus nebula.

REFERENCES

Abraham, Z.; Daminieli, A.; Durouchoux, P.; Nyman, L.; McAuliffe, F. 2002, IAUS, 206, 234.
“Maser effects in the recombination lines of Eta Carinae”

Brown, R. L.; Lockman, F. J.; Knapp, G. R. 1978, A&A, 16, 445-485. *“Radio recombination lines”*

Clark, J. S.; Larionov, V. M.; Arkharov, A. 2005, A&A, 435, 239-246. *“On the population of galactic Luminous Blue Variables”*

Cox, P.; Martin-Pintado, J.; Bachiller, R.; Bronfman, L.; Cernicharo, J.; Nyman, L.-A.; Roelfsema, P. R. 1995a, A&A, 295, L39-L42. *“Millimeter recombination lines towards Eta Carinae”*

Cox, P.; Mezger, P. G.; Sievers, A.; Najarro, F.; Bronfman, L.; Kreysa, E.; Haslam, G. 1995b, A&A, 297, 168-174. *“Millimeter emission of eta Carinae and its surroundings”*

Davidson, K. & Humphreys, R. M. 1997, ARA&A, 35, 1. *“Eta Carinae and its Environment”*

De Pree, C. G.; Wilner, D. J.; Mercer, A. J.; Davis, L. E.; Goss, W. M.; Kurtz, S. 2004, ApJ, Vol. 600, Issue 1, 286-291. *“Broad Recombination Line Objects in W49 North on 600 AU Scales”*

Dupree, A. K.; Goldberg, L. 1970, A&A, 8, 231. *“Radiofrequency Recombination Lines”*

Gomez, H. L.; Dunne, L.; Eales, S. A.; Edmunds, M. G. 2006, RAS, MNRAS 372, 1133–113.
“Submillimetre emission from η Carinae”

Gomez, H. L.; Vlahakis, C.; Stretch, C. M.; Dunne, L.; Eales, S. A.; Beelen, A.; Gomez, E. L.;

- Edmund, M. G. 2010, RAS, MNRAS 401, L48–L5. “*Edmunds Submillimetre variability of Eta Carinae: cool dust within the outer ejecta*”
- Gordon, M. A. & Sorochenko, R. L. (2009). “*Radio Recombination Lines: Their Physics and Astronomical Applications*”
- Güsten, R.; Nyman, L. Å.; Schilke, P.; Menten, K.; Cesarsky, C.; Booth, R. 2006, A&A, 454, L13-L16. “*The Atacama Pathfinder EXperiment (APEX) - a new submillimeter facility for southern skies -*”
- Ignace, R. 2009, AN, Vol. 330, Issue 7, p.717. “*Recombination lines and free-free continua formed in asymptotic ionized winds: Analytic solution for the radiative transfer*”
- Karttunen, H.; Kröger, P.; Oja, H.; Poutanen, M. & Donner, K. J. (2007). “*Fundamental Astronomy*” (5th edition).
- Kogure, T. & Leung, K.-C. (2007). “*The Astrophysics of Emission-Line Stars*”
- Oks, E. 2004, ApJ, Vol. 609, Issue 1, L25-L28. “*On the Puzzle of the Observed Narrowing of Radio Recombination Lines*”
- Osterbrock, D. E.; Ferland, G. J. (2006). “*Astrophysics of Gaseous Nebulae and Active Galactic Nuclei*” (2nd edition).
- Rodriguez, L. F. 1982, RmxA, 5:3, 179. “*On the Intensity and Shape of Radio Recombination Lines from Ionized Stellar Winds*”
- Scuderi, S.; Panagia, N.; Stanghellini, C.; Trigilio, C.; Umana, G. 1998, A&A, 332, 251-267. “*Radio observations of stellar winds from early type stars*”
- Smirnov, G. T.; Sorochenko, R. L.; Pankonin, V. 1984, A&A, Vol. 135, 116-121. “*Stark broadening in radio recombination lines towards the Orion Nebula*”

Smith, N. 2006, ApJ, 644, 1151-1163. *“The Structure of the Homunculus. I. Shape and Latitude Dependence from H₂ and [Fe II] Velocity Maps of Eta Carinae”*

Smith, N.; Davidson, K.; Gull, T. R.; Ishibashi, K.; Hillier, D. J. 2003a, ApJ, 586, 432-450. *“Latitude-dependent Effects in the Stellar Wind of η Carinae”*

Smith, N. & Ferland, G. J. 2007, ApJ, 655, 911-919. *“The Structure of the Homunculus. II. Modelling the Physical Conditions in Eta Carinae's Molecular Shell”*

Smith, N.; Gehrz, . D.; Hinz, P. M.; Hoffmann, W. F.; Hora, J. L.; Mamajek, E. E.; Meyer, M. R. 2003b, AJ, 125, 1458-1466. *“Mass and Kinetic Energy of the Homunculus Nebula around η Carinae”*

Shu, F. H. (1982). *“The Physical Universe: An Introduction to Astronomy”*

Soker, N. 2004, UCP, 612, 1060-1064. *“Why a Single-Star Model Cannot Explain the Bipolar Nebula of η Carinae”*

Walmsley, C. M. 1990, A&A, 82, 201-206. *“Level populations for millimeter recombination lines”*

Wilson, T. L.; Rohlfs, K.; Hüttemeister, S. (2009). *“Tools of Radio Astronomy”* (5th edition)